JOURNAL OF GUIDANCE, CONTROL, AND DYNAMICS
Vol. 24, No. 5, September–October 2001

Design of an Aeroelastic Delta Wing Model for Active Flutter Control

John A. Rule*
Active Control eXperts, Inc., Cambridge, Massachusetts 02142
and
Robert E. Richard† and Robert L. Clark‡
Duke University, Durham, North Carolina 27708

Ongoing research into the active control of aeroelastic structures has resulted in a new model for the control of delta wing flutter. An analytical and numerical formulation for both the aerodynamic forcing and structural response of the wing was developed. The order of the aerodynamic model was reduced through balanced model reduction, yielding an accurate, low-order representation of the three-dimensional flowfield around the delta wing. This fully coupled aero/structural model was used to investigate the optimal placement of piezoelectric sensors and actuators to design an adaptive structure that emphasized control of the flutter mode. Previous work has shown that such control schemes can delay the onset of flutter to increased dynamic pressure. This work extends the practical use of reduced-order aerodynamic modeling to the realm of real-time control system design, while simultaneously applying recently developed techniques for open-loop design and selection of sensors and actuators. Results indicate that a single sensor/actuator pair can be designed to significantly extend the flutter boundary.

Nomenclature

$\boldsymbol{A}, \boldsymbol{B}$	=	aerodynamic influence matrices
A_p	=	piezoelectric patch area
AR	=	wing aspect ratio
$\boldsymbol{C}_p$	=	piezoelectric capacitance
c	=	wing chord
D	=	wing displacement modeshape
d_{31}	=	piezoelectric strain constant
E_p	=	piezoelectric modulus
$\boldsymbol{F}$	=	aerodynamic force coefficient
$\boldsymbol{G}_{c,o}$	=	aerodynamic Gramian controllability/observability matrices
h	=	wing thickness
h_p	=	piezoelectric patch thickness
$\boldsymbol{K}$	=	structural stiffness matrix
$\boldsymbol{K}_p$	=	piezoelectric stiffness matrix
$\boldsymbol{M}$	=	structural stiffness matrix
$\boldsymbol{M}_p$	=	piezoelectric stiffness matrix
$\boldsymbol{q}$	=	piezoelectric charge
$\boldsymbol{R}$	=	generalized structural force
$\boldsymbol{r}$	=	generalized structural coordinate
s	=	wing span
$\boldsymbol{T}$	=	balancing transformation matrix
TR	=	wing taper ratio (tip chord/root chord)
U_∞	=	freestream velocity
u	=	normalized beam coordinate, chordwise
v	=	normalized beam coordinate, spanwise
$\boldsymbol{v}_p$	=	piezoelectric applied voltage
$\boldsymbol{w}$	=	normal wash on wing
x	=	wing physical coordinate, chordwise
y	=	wing physical coordinate, spanwise
Γ	=	vortex circulation
γ	=	balanced aerodynamic coordinates
δ	=	assumed spatial modeshape function
ε_1^S	=	piezoelectric dielectric constant
θ	=	electromechanical coupling matrix
κ	=	spanwise spatial wave number
ν_p	=	piezoelectric Poisson ratio
σ	=	chordwise spatial wave number
τ	=	dimensionless aerodynamic time
ϕ	=	spanwise assumed mode
ψ	=	chordwise assumed mode

Received 12 November 1999; revision received 17 January 2001; accepted for publication 20 January 2001.

*Senior R&D Engineer, 215 First Street. Member AIAA.
†Research Assistant, Department of Mechanical Engineering and Materials Science.
‡Professor, Department of Mechanical Engineering and Materials Science. Member AIAA.

Introduction

A COMBINATION of efforts is underway to create a computational and experimental model for the study of aeroelastic control. As each layer of complexity is added to the model, which must accurately capture the structural mechanics of a delta wing, the aerodynamic loads on that structure, the electromechanical behavior of surface-mounted piezoelectric sensors and actuators, and the implementation of a real-time adaptive control algorithm, real-time design constraints demand that each component of the model be reduced to its essential physics. To this end, work has progressed to achieve a low-order model that embodies the behavior of the true physical system for initial adaptive structure design.

The present research effort began with a focus on aerodynamic model reduction.[1] A summary of this issue can be stated as follows: The choice to spatially discretize the governing equations of fluid flow, whether linearized or full potential, Euler or Navier–Stokes, yields a remarkably inefficient representation of the flow from a computational standpoint. The number of degrees of freedom, or states, used to model the flow in this manner far exceeds the optimal number of well-chosen, spatially continuous, distributed states that might otherwise be used to represent the flow. Recent model reduction techniques focus on finding, or at least approaching, these optimal states.[2–6]

The first attempts to construct reduced-order aerodynamic models were based on standard eigenanalysis techniques.[2,3] Under the assumption that the discretized numerical model could be expressed as a generalized eigenvalue problem, the eigenmodes of the fluid were found. Model reduction was achieved by retaining only lightly damped modes, neglecting the rest. Unfortunately, accurate solutions required substantial numbers of modes to be retained, limiting the amount of reduction that could be achieved. More recent developments have focused on the use of proper orthogonal decomposition[7,8] or balanced realization[5,6,9–11] instead. Both techniques have at their heart a singular value decomposition that finds

the strongest path through the aerodynamic system between system inputs, typically wing or control surface motion, and system outputs, such as aerodynamic loads. The present analysis makes use of balanced realization to reduce the size of a three-dimensional, incompressible vortex lattice model from 1000 states down to roughly the number of structural states, in this study 50, used to model the delta wing.

A simple Ritz method is employed for the structural model of the delta wing, following the work of Andersen.[12] Sets of beam displacement functions are assumed in the chordwise (free–free) and spanwise (clamped–free) directions of a rectangular plate, with products of these functions giving the assumed displacement at any point on the wing. This plate is then mapped into a triangular domain. Mass and stiffnes matrix integrals are performed in a rectangular computational domain and converted to the triangular physical domain through an appropriate coordinate transformation. An additional transformation is employed to convert from the assumed structural modes to an approximation of the natural modes of the system, using standard eigenanalysis techniques. The formulation is sufficiently general that it can model plates of arbitrary constant taper, from rectangular all of the way down to triangular, and arbitrary aspect ratio. The present work deals only with the case of a right-trianglar delta wing.

The computational aeroelastic model outlined was used to perform control system design studies, with the goal of delaying the onset of wing flutter[13–15] to a higher flow velocity. The linear theory flutter boundary was identified, and piezoelectric sensors and actuators were placed on the wing based on an open-loop spatial optimization design procedure.[16–20] Under this procedure, many candidate sensors and actuators, of varying size, shape, and orientation, were placed on the wing. With piezomass and stiffness effects neglected, electromechanical coupling matrices were computed for all of the piezos.[21] An appropriate performance metric was chosen for flutter control, resulting in a sensor and actuator displaying maximum coupling to selected modes in the bandwidth of interest, with a penalty applied to out-of-bandwidth coupling.[19]

A controller was designed for operation at a flow velocity slightly below the linear flutter boundary. Closed-loop performance was then assessed based on the predicted increase in flutter velocity. The candidate sensor/actuator pair and controller discussed in this paper resulted in a 20% increase in predicted flutter velocity.

Theoretical Development

The fully coupled aeroelastic model with embedded piezoelectric sensors and actuators is developed hereafter as a series of state-space models. First, a simple structural model of the wing is developed based on the Ritz method (see Ref. 12). The structural model includes a brief review of the correct modeling of the electromechanical coupling between the piezoelectric sensors and actuators and the wing. Next, the unsteady aerodynamic equations governing the three-dimensional flow about the model delta wing are derived. Aerodynamic model reduction is discussed as a way to create an accurate, low-order representation of the flow. Finally, an outline is given of the open-loop design procedure used to select spatially optimal sensor and actuator locations for flutter control.

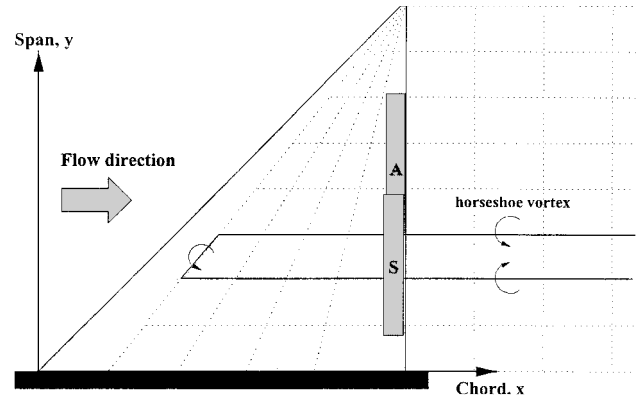

Fig. 1 Delta wing geometry with aerodynamic grid and sensor *S* and actuator *A* piezoelectric transducers.

With standard aerodynamic nomenclature, wing taper ratio is defined as the ratio of the wing tip chord over the root chord, and aspect ratio is defined in terms of root chord, span, and taper ratio as

$$\mathrm{AR} \equiv \frac{\text{span}^2}{\text{wing area}} = \frac{2}{1+\mathrm{TR}}\left(\frac{s}{c}\right) \tag{1}$$

To facilitate the use of clamped–free and free–free beam functions later on, any wing fitting the preceding description can be mapped to a unit square domain, referred to here as normalized beam coordinates. The transformations of Eq. (2) map any point on the wing from physical coordinates to normalized beam coordinates,

$$u = \frac{x/c - 2(1-\mathrm{TR})y/s}{1-2(1-\mathrm{TR})y/s}, \qquad v = \frac{2y}{s} \tag{2}$$

and a corresponding pair of inverse transformations maps them back,

$$x/c = u + (1-\mathrm{TR})(1-u)v, \qquad y/s = v/2 \tag{3}$$

For this study, a delta wing with 45-deg leading-edge sweep is considered, as shown in Fig. 1. This corresponds to a taper ratio of zero and an aspect ratio of four.

In accordance with the Ritz method, the total transverse displacement at any point on the wing can be expressed as a time-dependent weighted sum of assumed spatial mode shape functions,

$$D(x, y, t) = \sum_{n=1}^{N} \delta_n(x, y) r_n(t) \tag{4}$$

These spatial shape functions are in turn products of assumed beam modes in the chordwise and spanwise directions:

$$\delta_n(x, y) = \psi_{i(n)}[u(x, y)] \times \phi_{j(n)}[v(x, y)] \tag{5}$$

where $\psi_i(u)$ are the one-dimensional free–free beam modes in the chordwise direction of the plate,

$$\psi_i(u) = \begin{cases} 1 & i = 1 \\ \sqrt{3}(1-2u) & i = 2 \\ [\cos(\sigma_i u) + \cosh(\sigma_i u)] - \left[\dfrac{\cos(\sigma_i) - \cosh(\sigma_i)}{\sin(\sigma_i) - \sinh(\sigma_i)}\right][\sin(\sigma_i u) + \sinh(\sigma_i u)] & i \geq 3 \end{cases} \tag{6}$$

and $\phi_j(v)$ are the one-dimensional clamped–free beam modes in the spanwise direction,

$$\phi_j(v) = -[\cos(\kappa_j v) - \cosh(\kappa_j v)] - \left[\frac{\sin(\kappa_j) - \sinh(\kappa_j)}{\cos(\kappa_j) + \cosh(\kappa_j)}\right] \times [\sin(\kappa_j v) - \sinh(\kappa_j v)] \qquad j \geq 1 \tag{7}$$

These functions are orthonormal over the range $0 < u, v < 1$ and have associated wave numbers given in Table 1.

Delta Wing Structural Model

The delta wing model under consideration is assumed to behave as a thin plate of uniform mass and stiffness. The following general formulation allows for the treatment of a whole family of rectilinear wings of arbitrary constant taper ratio and aspect ratio through the use of a transformation to normalized beam mode coordinates, defined hereafter.

Table 1 Approximate spatial wave numbers for free–free and clamped–free beam modes

i	σ_i	j	κ_j
3	4.7300407	1	1.8751041
4	7.8532046	2	4.6940911
5	10.995608	3	7.8547574
≥ 6	$(\pi/2)(2i+1)$	≥ 4	$(\pi/2)(2j-1)$

With a standard application of Lagrange's equations (see Ref. 22) using the assumed mode shapes of Eqs. (5–7), a system of linear equations governing the motion of the wing results,

$$\boldsymbol{M}\ddot{\boldsymbol{r}} + \boldsymbol{K}\boldsymbol{r} = \boldsymbol{R} \tag{8}$$

The integrals that define the mass and stiffness matrices are most easily evaluated in normalized beam coordinates. In these coordinates, the domain of integration is square, with limits from zero to one in both directions.

Piezoelectric patches are added to the structural model of Eq. (8) following a method first suggested by Hagood, et al. in Ref. 21. Considerable simplification of the necessary mathematics exists for the case of rectangular surface-mounted patches with an electric field applied normal to the surface.[22] For this case, an electromechanical coupling matrix results for each patch,

$$\Theta = \frac{d_{31}E_p}{1-\nu_p}\left(\frac{h+h_p}{2c^2}\right)\int_{x_1}^{x_2}\int_{y_1}^{y_2}\left[\frac{\partial^2\delta_n(x,y)}{\partial^2 x} + \frac{\partial^2\delta_n(x,y)}{\partial^2 y}\right]\mathrm{d}x\,\mathrm{d}y \tag{9}$$

Each piezoelectric patch will contribute additional mass and stiffness to the structure as well. Under the assumption that the electric field across each piezo takes the form of an applied voltage, the new structural system, with piezoelectric actuators is

$$(\boldsymbol{M}+\boldsymbol{M}_p)\,\ddot{\boldsymbol{r}} + (\boldsymbol{K}+\boldsymbol{K}_p)\,\boldsymbol{r} = \boldsymbol{R} + \Theta\boldsymbol{v}_p \tag{10}$$

If these same piezoelecctric patches are used as secsors, the measured charge is given by

$$\boldsymbol{q} = \Theta^T\boldsymbol{r} + \boldsymbol{C}_p\boldsymbol{v}_p \tag{11}$$

where the piezoelectriccapacitanceis defined for each patch in terms of patch area, thickness, and dielectric constant as $C_p = \varepsilon_1^S A_p/h_p$.

A complete state-space structural model of the delta wing, with piezoelectric voltages and generalized modal forces as inputs and piezoelectriccharges, modal position, and modal velocity as outputs, is given by

$$\begin{Bmatrix}\dot{r}\\ \ddot{r}\\ \hline q\\ r\\ \dot{r}\end{Bmatrix} = \left[\begin{array}{cc|cc} \boldsymbol{0} & \boldsymbol{I} & \boldsymbol{0} & \boldsymbol{0}\\ -\hat{\boldsymbol{M}}^{-1}\hat{\boldsymbol{K}} & \boldsymbol{0} & -\hat{\boldsymbol{M}}^{-1}\Theta & -\hat{\boldsymbol{M}}^{-1}\\ \hline \Theta^T & \boldsymbol{0} & \boldsymbol{C}_p & \boldsymbol{0}\\ \boldsymbol{I} & \boldsymbol{0} & \boldsymbol{0} & \boldsymbol{0}\\ \boldsymbol{0} & \boldsymbol{I} & \boldsymbol{0} & \boldsymbol{0}\end{array}\right]\begin{Bmatrix}\boldsymbol{r}\\ \dot{\boldsymbol{r}}\\ \hline \boldsymbol{v}_p\\ \boldsymbol{R}\end{Bmatrix} \tag{12}$$

This structural model has been validated against the classical results of Ref. 23 for a variety of rectangular, tapered, and triangular plates, including the delta wing configuration under consideration here.

Baseline Aerodynamic Model

The aerodynamic method used for discussion purposes here is the unsteady, incompressible vortex lattice method developed by Hall in Ref. 2. The details of that formulation will not be repeated here due to length considerations, but it will be assumed that the appropriate discrete-time aerodynamic influence matrices have been constructed as a starting point. Refer back to Fig. 1, which shows the aerodynamic grid laid on top of the delta wing plate. The wing is assumed to be symmetric about the midspan, $y = 0$, and this symmetry is accounted for in the aerodynamic influence matrices discussed hereafter.

In general, the strengths of the vortices modeling the flow about the wing at time $n+1$ are related to the vortex strengths at time n and the normal wash on the wing at the mid-time step $n+\frac{1}{2}$ by a pair of aerodynamic influence matrices as follows:

$$\boldsymbol{A}\{\boldsymbol{\Gamma}/U_\infty c\}^{n+1} + \boldsymbol{B}\{\boldsymbol{\Gamma}/U_\infty c\}^{n} + \{\boldsymbol{w}/U_\infty\}^{n+\frac{1}{2}} = 0 \tag{13}$$

For simplicity, restrict the system input, which in this case is the normal wash on the wing, to be a function of wing assumed modal displacement and velocity only,

$$\begin{Bmatrix}\boldsymbol{w}\\ \hline U_\infty\end{Bmatrix}^{n+\frac{1}{2}} \equiv \boldsymbol{W}\begin{Bmatrix}\boldsymbol{r}/c\\ \dot{\boldsymbol{r}}/U_\infty\end{Bmatrix} \tag{14}$$

Vortex lattice methods typically require a discrete-time formulation, as can be seen in Eq. (13). This is partly due to restrictions on vortex spacing, which must be uniform in the chordwise direction, fixing the wake convection time step to the grid spacing. Rather than accepting these limitations, it is convenient to convert to a continuous time model via a series expansion,

$$\boldsymbol{\Gamma}^n = \boldsymbol{\Gamma}^{n+\frac{1}{2}} + \left(-\frac{\Delta\tau}{2}\right)\frac{\mathrm{d}\boldsymbol{\Gamma}^{n+\frac{1}{2}}}{\mathrm{d}\tau} + \cdots$$

$$\boldsymbol{\Gamma}^{n+1} = \boldsymbol{\Gamma}^{n+\frac{1}{2}} + \left(-\frac{\Delta\tau}{2}\right)\frac{\mathrm{d}\boldsymbol{\Gamma}^{n+\frac{1}{2}}}{\mathrm{d}\tau} + \cdots \tag{15}$$

where $\tau \equiv U_\infty t/c$ is the standard dimensionless aerodynamic timescale. The constant $\Delta\tau$ is set by the aerodynamic grid resolution. After substitution of Eq. (15) into Eq. (13) and some manipulation, the following system results:

$$\begin{aligned}\frac{\mathrm{d}}{\mathrm{d}\tau}\begin{Bmatrix}\boldsymbol{\Gamma}\\ \hline U_\infty c\end{Bmatrix} &= -\frac{2}{\Delta\tau}[\boldsymbol{A}-\boldsymbol{B}]^{-1}[\boldsymbol{A}+\boldsymbol{B}]\begin{Bmatrix}\boldsymbol{\Gamma}\\ \hline U_\infty c\end{Bmatrix}\\ &\quad -\frac{2}{\Delta\tau}[\boldsymbol{A}-\boldsymbol{B}]^{-1}\boldsymbol{W}\begin{Bmatrix}\boldsymbol{r}/c\\ \dot{\boldsymbol{r}}/U_\infty\end{Bmatrix}\\ &\equiv \boldsymbol{A}'\begin{Bmatrix}\boldsymbol{\Gamma}\\ \hline U_\infty c\end{Bmatrix} + \boldsymbol{B}'\begin{Bmatrix}\boldsymbol{r}/c\\ \dot{\boldsymbol{r}}/U_\infty\end{Bmatrix}\end{aligned} \tag{16}$$

Note that the time index, $n+\frac{1}{2}$, is no longer necessary and has been dropped.

The generalized aerodynamic forces are calculated by integrating the product of the surface pressure on the wing times each assumed mode shape over the wing surface,

$$R_n = \int\!\!\int \Delta p(x,y)\delta_n(x,y)\,\mathrm{d}x\,\mathrm{d}y \tag{17}$$

where pressure is calculated from the vortex strengths using the linearized Bernoulli equation,

$$\frac{\Delta p(x,y)}{\rho_\infty} = \frac{\partial\boldsymbol{\Gamma}}{\partial t} + U_\infty\frac{\partial\boldsymbol{\Gamma}}{\partial x} \tag{18}$$

After some standard manipulations,[24] the generalized forces on the wing can be written as a vector of aerodynamic coefficients

$$\hat{\boldsymbol{R}} \equiv \frac{\boldsymbol{R}}{1/2\rho_\infty U_\infty^2 S} = \boldsymbol{F}_1\begin{Bmatrix}\boldsymbol{\Gamma}\\ \hline U_\infty c\end{Bmatrix} + \boldsymbol{F}_2\frac{\mathrm{d}}{\mathrm{d}\tau}\begin{Bmatrix}\boldsymbol{\Gamma}\\ \hline U_\infty c\end{Bmatrix} \tag{19}$$

There is now sufficient information to create an aerodynamic state-space model,

$$\begin{Bmatrix}(\mathrm{d}/\mathrm{d}\tau)\{\boldsymbol{\Gamma}/U_\infty c\}\\ \hline \hat{\boldsymbol{R}}\end{Bmatrix} = \left[\begin{array}{c|c}\boldsymbol{A}' & \boldsymbol{B}'\\ \hline \boldsymbol{F}_1+\boldsymbol{F}_2\boldsymbol{A}' & \boldsymbol{F}_2\boldsymbol{B}'\end{array}\right]\begin{Bmatrix}\boldsymbol{\Gamma}/U_\infty c\\ \hline \boldsymbol{r}/c\\ \dot{\boldsymbol{r}}/U_\infty\end{Bmatrix} \tag{20}$$

There are several important points to note here. First, all of the quantities in the aerodynamic state-space model are nondimensional, as is traditional in aerodynamic analyses. As a consequence, manipulations of the model, such as the model reduction technique that is about to be discussed, are independent of flow velocity U_∞ and need only be performed once for a given

wing geometric configuration. Care must be taken when coupling this model to the structural model of the preceding section, which was constructed with dimensional force inputs and dimensional position and velocity outputs. Also, the structural and aerodynamic timescales differ between Eq. (12) and Eq. (20), by the constant factor U_∞/c.

Reduced-Order Aerodynamic Model

For a typical calculation using the model of the preceding section, one might choose to represent the aerodynamics about the wing with a vortex lattice consisting of 8 chordwise by 10 spanwise vortices, and track 4 chords of wake of the same lattice density. This translates to a 400-state model for the aerodynamics alone, without accounting for the states due to the structural model or controller. Note that this is a very low grid density. Flutter calculations would typically require only the first few dozen natural structural modes, or on the order of 50 additional states. The dynamic compensator used for control would be expected to have even fewer states because only a single mode destabilizes the aeroelastic system. For design purposes, the size of the aerodynamic state-space model is unacceptable and provides the necessary motivation to consider balanced model reduction.

Aerodynamic systems provide an ideal opportunity for the application of balanced model reduction[5,6] because it is frequently the case that a large number of states must be used to transmit information from a small number of inputs (system geometry, surface position, and velocity), to a small number of outputs (net lift, generalized forces on each structural mode), which is exactly the case here. From a systems point of view, the details of the flow are unimportant; the aerodynamics are simply providing a transmission path from wing geometry to forces. Creating a balanced realization of this system requires the application of a similarity transformation such that the resulting system controllability and observability gramians (see Ref. 25) are equal and diagonal.[10] Such a system is said to be internally balanced.

Under the assumption that a transformation matrix exists such that

$$\left.\begin{aligned} \boldsymbol{G}_c' &= \boldsymbol{T}\boldsymbol{G}_c\boldsymbol{T}^T \\ \boldsymbol{G}_o' &= \boldsymbol{T}^{-T}\boldsymbol{G}_o\boldsymbol{T}^{-1} \end{aligned}\right\} \qquad \boldsymbol{G}_c' = \boldsymbol{G}_o' = \mathrm{diag}(\lambda) \tag{21}$$

the balanced aerodynamic state-space model now takes the form

$$\left\{\begin{array}{c} (\mathrm{d}/\mathrm{d}\tau)\{\gamma/U_\infty c\} \\ \hat{\boldsymbol{R}} \end{array}\right\} = \left[\begin{array}{c|c} \tilde{\boldsymbol{A}} & \tilde{\boldsymbol{B}} \\ \hline \tilde{\boldsymbol{C}} & \boldsymbol{F}_2\boldsymbol{B}' \end{array}\right] \left\{\begin{array}{c} \gamma/U_\infty c \\ \boldsymbol{r}/c \\ \dot{\boldsymbol{r}}/U_\infty \end{array}\right\} \tag{22}$$

where

$$\gamma = \boldsymbol{T}\,\boldsymbol{\Gamma}, \qquad \tilde{\boldsymbol{A}} = \boldsymbol{T}\boldsymbol{A}'\boldsymbol{T}^{-1}, \qquad \tilde{\boldsymbol{B}} = \boldsymbol{T}\boldsymbol{B}'$$

$$\tilde{\boldsymbol{C}} = [\boldsymbol{F}_1 + \boldsymbol{F}_2\boldsymbol{A}']\boldsymbol{T}^{-1} \tag{23}$$

The primary benefit of the system in this form is that the diagonal elements of the balanced gramian matrix, defined in Eq. (21), now provide an indication of the relative importance of a particular state to the system input/output path. Large values of $\boldsymbol{\lambda}$ indicate states that are both highly controllable and highly observable, whereas smaller values signify states that are neither very controllable nor observable. In the present context, the first few states provide the strongest transmission path through the aerodynamics from the structural inputs of delta wing position and velocity to the generalized forces acting on the wing. Algorithms are available, for example, balreal( ) in MATLAB®,[26] for finding the transformation matrix $\boldsymbol{T}$. This is computationally expensive, but must be done only once during the design process.

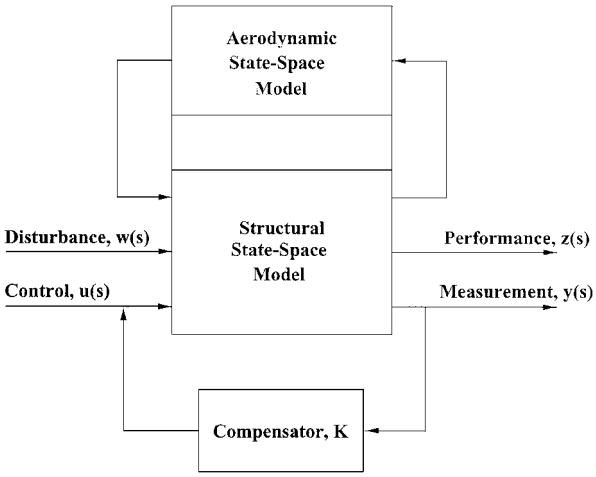

Fig. 2 Block diagram of coupled aeroelastic model cast in two-port form for controller design.

Control System Design

An earlier section detailed the method for incorporating piezoelectric sensors and actuators into the structural model for control. The choice of placement of those sensors and actuators and the design of an appropriate compensator for aeroelastic flutter control are the topics of this section. To begin, consider the block diagram of the coupled aeroelastic system, presented in Fig. 2. The system has been cast here in two-port form.[22] Note that the aerodynamics simply act as a flow-speed-dependent feedback loop to the structural system.

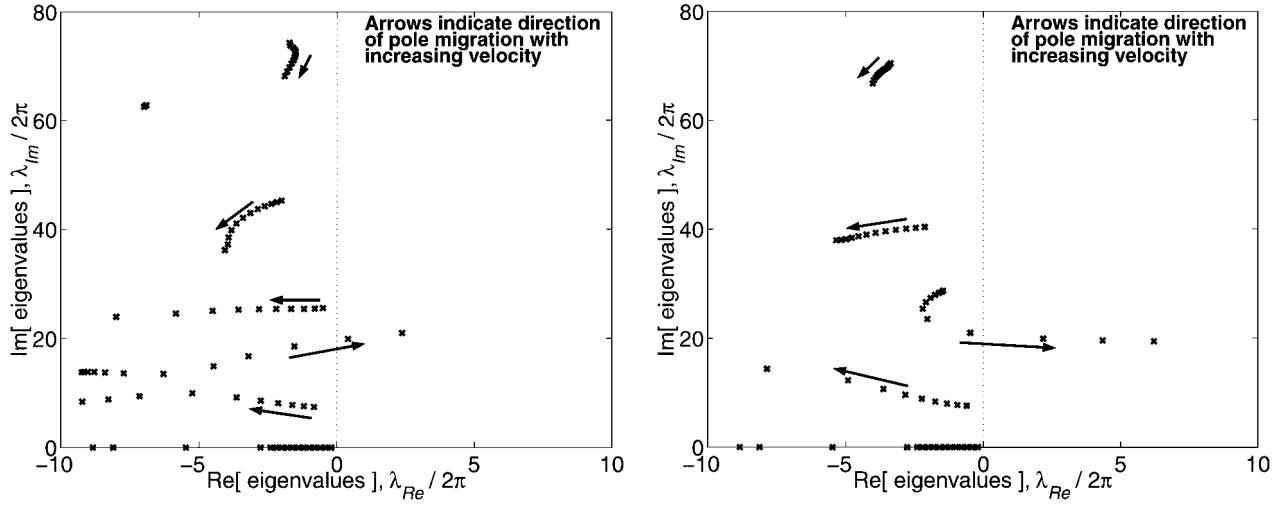

Fig. 3 Open-loop (left) and closed-loop (right) poles at 5-m/s increments from 5 to 60 m/s.

A representative model delta wing (see Table 2 for physical parameters) was determined to have a linear flutter speed of 45 m/s, with the instability occurring in the second aeroelastic mode (see Fig. 3 for open- and closed-loop poles over a range of flow velocities.) A disturbance input was constructed to excite the first 15 modes of the structure at just below this operating condition. The performance metric was chosen to be a weighted combination of the first 15 modal velocities. With the open-loop spatial optimization technique of Smith and Clark,[20] an assortment of 726 candidate sensors and actuators were distributed over the surface of the wing, and the electromechanical coupling matrix for each was computed. All of the candidate patches were assumed to be 0.2-mm-thick single sheet lead zirconate titanate (PZT) from Piezo Systems, Inc. The trial patch set consisted of patches of the following discrete sizes: 1×6, 1.5×4, 2×3, 3×2, 4×1.5, and 6×1 in. Note that all patches have an area of six in.^{2} and that the repeating of the dimensions reflects the two possible orientations of each patch relative to the wing chord. The candidates were overlapped by an automatic placement algorithm to provide complete coverage of the wing, resulting in approximately equal numbers of each size.

Table 2 Physical parameters of model delta wing

Parameter	Value
Chord	0.381 m (15 in.)
Semispan	0.381 m
Thickness	0.794×10^{-3} m
Density	3.36×10^{3} Kg/m^3
Young's modulus	71.0×10^{9} N/m^2

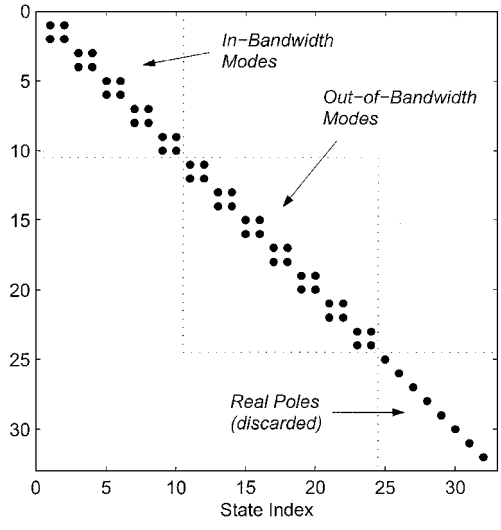

Fig. 4 System matrix demonstrating classification of in-bandwidth and out-of-bandwidth modes and real poles.

With an algorithm first employed by Lim[1] and Gawronski,[16] the approximate Hankel singular values (HSVs) were estimated from a discrete time representation of the open-loop ($K = 0$), coupled aeroelastic system. The HSVs can be used to determine the open-loop controllability and observability gramians and provide an effective measure of the sensor or actuator's ability to couple to particular modes of the system. The goal, of course, is to find a sensor/actuator pair that strongly couples to a select few modes within the bandwidth of interest (here, below 200 Hz) and exhibits limited coupling to out-of-bandwidth modes, providing a natural rolloff of the control loop with frequency. The advantage of the Lim and Gawronski method is that it does not require a full singular value decomposition of the system, which could be computationally expensive, but instead relies on the assumption of lightly damped complex modes in the system to estimate the HSVs. Again, following Smith and Clark,[20] a modal selection vector was chosen to emphasize coupling to the first four structural modes. The optimal sensor to actuator pair was selected from $(726 \times 726)/2 = 263,538$ unique possible combinations in just a few seconds on a desktop personal computer.

A simplified system matrix in modal coordinates is provided in Fig. 4 for illustration purposes. Note that the system has been divided into three zones: in bandwidth, out of bandwidth, and real poles. The method of Lim and Gawronski[16] is only valid for lightly damped, complex poles. Thus, the real poles, which in this case correspond to the heavily damped aerodynamic states, are truncated prior to performing the HSV estimates. The performance metric rewards coupling to modes that are in bandwidth and penalizes coupling to modes that are out of bandwidth. The resulting spatially optimal sensor/actuator pair are shown in Fig. 1.

The final step in model construction was compensator design. H_2-synthesis was used to design a controller at a single flow condition just below the flutter velocity. With reference to the two-port block diagram of Fig. 2, the disturbance and performance metrics that were used for actuator selection were used for controller design. The control input was the single spatially optimal actuator, and the measurement was the corresponding optimal sensor. In addition, both process noise and sensor noise were included as additional disturbance inputs, as is typical of linear quadratic Gaussian design,[27,28] and the performance path was augmented by a control effort penalty. The cost function was constructed from the square of the two-norm between the performance (error) z and the

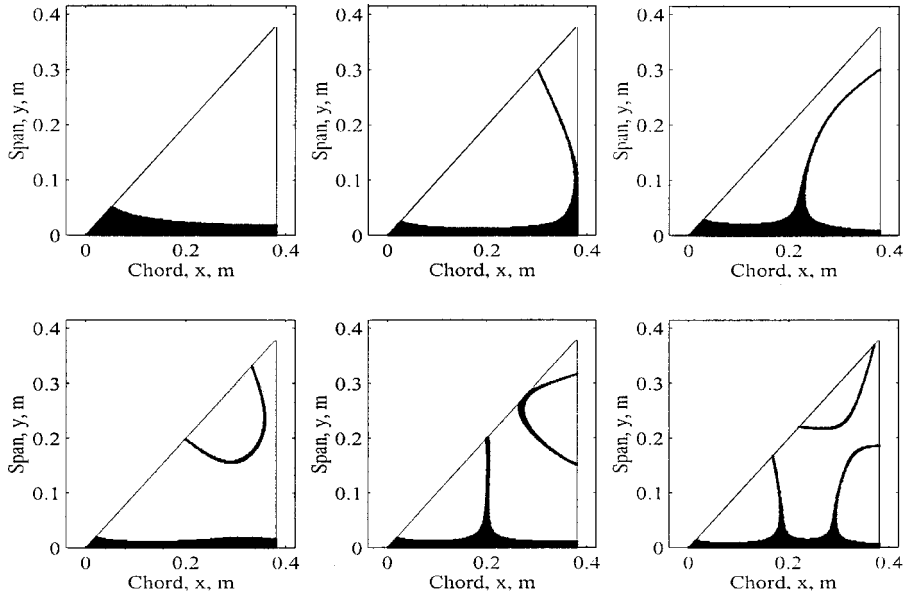

Fig. 5 Nodal lines of first six natural vibrational modes of a right triangular plate (clamped along x axis).

disturbance w. The cost function can be expressed mathematically as follows:

$$J = \lim_{t \to \infty} \boldsymbol{E}[z^T(t)z(t)] = \|T_{zw}\|_2^2 \tag{24}$$

where T_{zw} is the closed-loop transfer function between z and w. The design process resulted in a 25-state compensator. This compensator was then used over a range of flow velocities to evaluate closed-loop system performance.

Results and Discussion

Extensive work was done to validate both the structural and aerodynamic models independently, before coupling them together. The work of Leissa[23] regarding the vibration of plates, including a right-triangular wing, was used to check the accuracy of the assumed modes plate model given by Eq (12). Both natural frequencies and computed natural mode shapes compared favorably between the computational model and the experimentally tabulated results on page 219 of Ref. 23. The first six modes are shown in Fig. 5 for comparison. The authors have found it helpful to refer to these nodal line plots when assessing sensor and actuator placement schemes on the wing structure.

The aerodynamic model reduction technique was checked for accuracy by running several classical unsteady aerodynamics problems with both the full- and reduced-order models. Rule et al. demonstrated in Ref. 6 that the balanced aerodynamic states in a two-dimensional flow can be related to analytical potential flow solutions. Work is ongoing to address this issue with regard to the delta wing. For the problem at hand, the important question is the amount of model reduction that is achieved using the balanced realization technique. The values of the internally balanced gramian matrix for the aerodynamic system, defined in Eq. (21), are plotted in Fig. 6. Recall that these values provide a measure of the importance of the corresponding state to the input/output path of interest. Furthermore, the cumulative sum of a subset of gramian values can be used to determine the fractional contribution of that subset to the controllability (or observability) of the full model. This provides a convenient criterion for retaining or neglecting states. A conservative cutoff criterion requiring the reduced model to retain 99.9% of the controllability of the full model was employed in this study. This resulted in a reduced-order aerodynamic model of only 40 states, as indicated in Fig. 6. This is exactly 10% of the original 400 states, with only a 0.1% loss of accuracy.

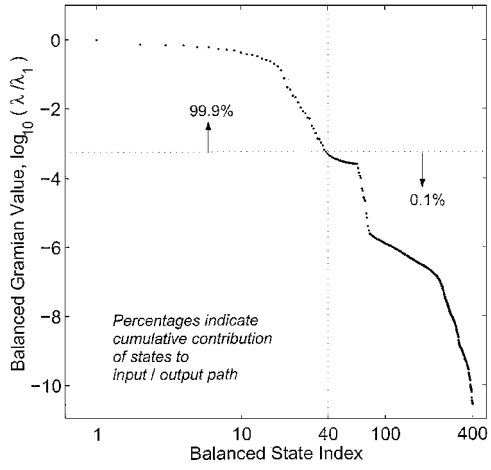

Fig. 6 Controllability/observability Gramian resulting from aerodynamic system balancing.

Next, characterization of the open-loop aeroelastic system was carried out before starting the controller design process. With the test configuration of Table 2, the system eigenvalues were examined over a range of flow velocities from 5 to 60 m/s. A root locus of these values is plotted in Fig. 3. In Fig. 3, the modes that are predominantly structural appear as densely packed lines that originate at each of the first five natural frequencies of the wing (7.6, 29, 41, 71, and 96 Hz). The aerodynamics have the effect of causing pole migration, modifying both the frequency and damping ratio of each mode. The system goes unstable when the pole associated with the second structural mode crosses into the right half-plane at approximately 45 m/s. The remaining sparsely distibuted poles in Fig. 3 are primarily associated with the aerodynamics; they move radially away from the origin, exhibiting a linear variation in frequency with velocity, as shown in Ref. 1.

After the selection of the spatially optimal sensor/actuator pair based on modal coupling near the flutter boundary, a compensator was designed to stabilize the system. The success of this controller design was evaluated by comparing the open- and closed-loop frequency response in the disturbance-to-performance path at the design point, as shown in Fig. 7. In Fig. 7, the open-loop resonant peak clearly dominates the system response, whereas in the closed-loop system, the instability has been eliminated. The off-design performance of the controller was satisfying as well; the system remained stable, though with little performance, at low velocity. Above the design point, the closed-loop system is stable up to a velocity of 54 m/s, which represents a 20% increase in the flutter boundary.

Conclusions

A model was developed to investigate the aeroelastic behavior and active control of a family of thin rectilinear wings of arbitrary aspect ratio and taper ratio. Performance of this model has been detailed here for the case of a right-triangular delta wing. The

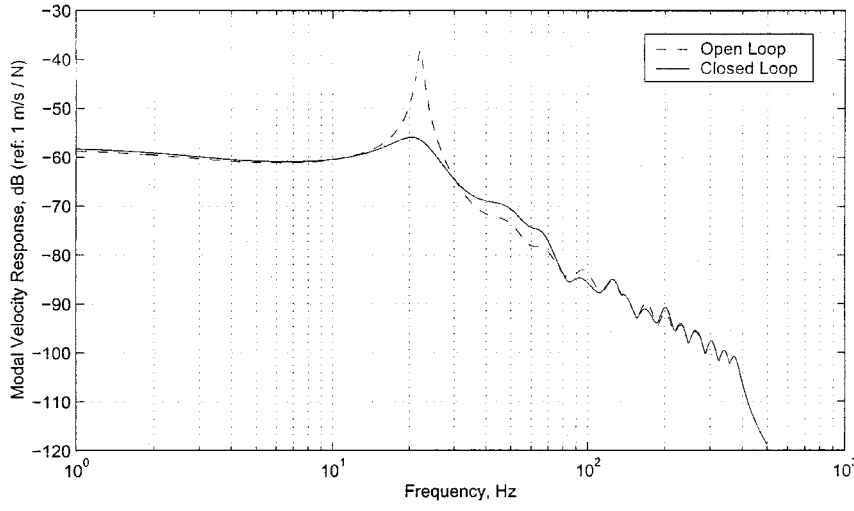

Fig. 7 Maximum singular values in the disturbance (modal forcing) to performance (modal velocity) path of the open- and closed-loop systems at the nominal design condition.

fully coupled model incorporated the use of balanced realization for aerodynamic model reduction, resulting in an accurate, computationally efficient model only 10% the size of the baseline aerodynamic model. A new spatial optimization technique was employed for sensor and actuator placement, resulting in a 20% increase in the flutter boundary of the system. The model provides a fast, accurate way to investigate various adaptive structural wing designs for control. Results from this study serve to demonstrate that adaptive structures can be designed to facilitate control. Furthermore, through design, preformance can be directed at specific structural modes, simplifying the resulting system.

Acknowledgments

This research was supported by the Air Force Office of Scientific Research under Grants F49620-98-1-0383 and F49620-96-1-0385, with Brian Sanders serving as Technical Monitor. The authors would like to thank Earl H. Dowell for many helpful discussions regarding aeroelastic behavior and Kenneth C. Hall for his insight on reduced-order aerodynamic modeling.

References

[1]Dowell, E. H., Hall, K. C., and Romanowski, M. C., "Eigenmode Analysis in Unsteady Aerodynamics: Reduced Order Models," *Applied Mechanics Review*, Vol. 50, No. 6, 1997, pp. 371–386.

[2]Hall, K. C., "Eigenanalysis of Unsteady Flows About Airfoils, Cascades, and Wings," *AIAA Journal*, Vol. 32, No. 12, 1994, pp. 2426–2432.

[3]Dowell, E. H., "Eigenmode Analysis in Unsteady Aerodynamics: Reduced-Order Models," *AIAA Journal*, Vol. 34, No. 8, 1996, pp. 1578–1583.

[4]Romanowski, M. C., and Dowell, E. H., "Reduced-Order Euler Equations for Unsteady Aerodynamic Flows: Numerical Techniques," AIAA Paper 96-0528, Jan. 1996.

[5]Baker, M., "Model Reduction of Large, Sparse, Discrete Time Systems with Application to Unsteady Aerodynamics (Finite Element, Lyapunov Equations)," Ph.D. Dissertation, Univ. of California, Los Angeles, CA, May 1996.

[6]Rule, J. A., Cox, D. E., and Clark, R. L., "Aerodynamic Model Reduction Through Balanced Realization," *AIAA Journal* (to be published).

[7]Florea, R., Hall, K. C., and Cizmas, P. G. A., "Reduced-Order Modeling of Unsteady Viscous Flows in a Compressor Cascade," *AIAA Journal*, Vol. 36, No. 6, 1998, pp. 1039–1048.

[8]Romanowski, M. C., "Reduced-Order Unsteady Aerodynamic and Aeroelastic Models Using Karhunen–Loève Eigenmodes," AIAA Paper 96-3981, Sept. 1996.

[9]Baker, M. L., Mingori, D. L., and Goggin, P. J., "Approximate Subspace Iteration for Constructing Internally Balanced Reduced-Order Models of Unsteady Aerodynamic Systems," *Proceedings of the 37th AIAA/ASME/ASCE/ASC Structures, Structural Dynamics, and Materials Conference*, AIAA, Reston, VA, 1996, pp. 1070–1085.

[10]Moore, B. C., "Principal Component Analysis in Linear Systems: Controllability, Observability, and Model Reduction," *IEEE Transactions on Automatic Control*, Vol. AC-26, No. 1, 1981, pp. 17–32.

[11]Laub, A. J., Heath, M. T., Paige, C. C., and Ward, R. C., "Computation of System Balancing Transformations and Other Applications of Simultaneous Diagonalization Algorithms," *IEEE Transactions on Automatic Control*, Vol. AC-32, No. 1, 1987, pp. 115–122.

[12]Andersen, B. W., "Vibration of Triangular Cantilever Plates by the Ritz Method," *Journal of Applied Mechanics*, Dec. 1954, pp. 365–370.

[13]Theodorsen, T., "General Theory of Aerodynamic Instability and the Mechanism of Flutter," NACA TR 496, 1935.

[14]Bisplinghoff, R. L., Ashley, H., and Halfman, R. L., *Aeroelasticity*, Addison Wesley Longman, Reading, MA, 1955, pp. 527–626.

[15]Dowell, E. H., *A Modern Course in Aeroelastcity*, Kluwer Academic, Dordrecht, The Netherlands, 1989, Chap. 2.

[16]Lim, K. B., and Gawronski, W., "Hankel Singular Values of Flexible Structures in Discrete Time," *Journal of Guidance, Control, and Dynamics*, Vol. 19, No. 6, 1996, pp. 1370–1377.

[17]Gawronski, W., and Lim, K. B., "Balanced Actuator and Sensor Placement for Flexible Structures," *International Journal of Control*, Vol. 65, No. 1, 1996, pp. 131–145.

[18]Lim, K. B., "Disturbance Rejection Approach to Actuator and Sensor Placement," *Journal of Guidance, Control, and Dynamics*, Vol. 20, No. 1, 1997, pp. 202–204.

[19]Clark, R. L., and Cox, D. E., "Band-Limited Actuator and Sensor Selection for Disturbance Rejection," *Journal of Guidance, Control, and Dynamics*, Vol. 22, No. 5, 1999, pp. 740–743.

[20]Smith, G. C., and Clark, R. L., "Adaptive Structure Design Through Optimal Spatial Compensation," *Proceedings of Active-99*, Noise Control Foundation, Poughkeepsie, NY, 1999, pp. 1013–1024.

[21]Hagood, N. W., Chung, W. H., and von Flotow, A., "Modelling of Piezoelectric Actuator Dynamics for Active Structural Control," *Proceedings of the 31st AIAA/ASME/ASCE/AHS Structures, Structural Dynamics, and Materials Conference*, AIAA, Washington, DC, 1990, pp. 2242–2256.

[22]Clark, R. L., Saunders, W. R., and Gibbs, G. P., *Adaptive Structures*, Wiley, New York, 1998, pp. 27–30.

[23]Leissa, A. W., *Vibration of Plates*, Acoustical Society of America, Sewickley, PA, 1993, pp. 195–200.

[24]Katz, J., and Plotkin, A., *Low Speed Aerodynamics, From Wing Theory to Panel Methods*, McGraw–Hill Series in Aeronautical and Aerospace Engineering, McGraw–Hill, New York, 1991, pp. 421–435.

[25]Skogestad, S., and Postlewaite, I., *Multivarible Feedback Control*, Wiley, Chichester, England, U.K., 1996, pp. 122–126.

[26]*MATLAB Control System Toolbox User's Guide*, Vol. 4, MathWorks, Inc., Natick, MA, 1998, pp. 11-16–11-18.

[27]Hong, J., and Bernstein, D. S., "Bode Integral Constraints, Colocation, and Spillover in Active Noise and Vibration Control," *IEEE Transactions on Control System Technology*, Vol. 6, 1998, pp. 111–120.

[28]Doyle, J. C., Glover, K., Khargonekar, P. P., and Francis, B. A., "State-Space Solutions to Standard H_2 and H_∞ Control Problems," *IEEE Transactions on Automatic Control*, Vol. 34, No. 8, 1989, pp. 831–847.